SAE TECHNICAL PAPER SERIES

2008-01-0808

Impact of Ceramic Substrate Web Thickness on Emission Light-Off, Pressure Drop, and Strength

Susan C. Lauderdale, Seth T. Nickerson, Jonathan D. Pesansky and Charles M. Sorensen
Corning Incorporated

Reprinted From: Advanced Catalysts & Substrates, 2008 (SP-2198)

ISBN 978-0-7680-1635-2

9 780768 016352

**2008 World Congress
Detroit, Michigan
April 14-17, 2008**

SAE International™

400 Commonwealth Drive, Warrendale, PA 15096-0001 U.S.A. Tel: (724) 776-4841 Fax: (724) 776-0790 Web: www.sae.org

All SAE papers, standards, and selected books are abstracted and indexed in the Global Mobility Database.

ISSN 0148-7191

Printed in USA

2008-01-0808

Impact of Ceramic Substrate Web Thickness on Emission Light-Off, Pressure Drop, and Strength

Susan C. Lauderdale, Seth T. Nickerson, Jonathan D. Pesansky and Charles M. Sorensen
Corning Incorporated

ABSTRACT

The effect of web thickness on emission performance, pressure drop, and mechanical properties was investigated for a series of catalyzed ceramic monolith substrates having cell densities of 900, 600 and 400 cpsi. As expected, thinner webs provide better catalyst light off performance and lower pressure drop, but mechanical strength generally decreases as web thickness is reduced. Good correlations were found between emission performance and geometric parameters based on bare and coated parts. An improved method for estimating the effects of cell density and web thickness on bare substrate strength is described, and the effect of porosity on material strength is also examined. New mechanical strength correlations for ceramic honeycombs are presented. The availability of a range of ceramic product geometries provides options for gasoline exhaust emission design and optimization, especially where increased levels of performance are desired.

INTRODUCTION

The cellular geometry of ceramic honeycomb substrates is a critical design element that affects product performance. Theoretical relationships of cell density and web thickness to product performance have been well documented, as have numerous experimental studies. In principle any combination of cell density and web thickness is possible, but various practical constraints such as manufacturability, strength, durability, and canning have limited product availability to those having the best combination of attributes. Nevertheless, aftertreatment technology continues to demand higher performance substrates to match the needs in the market.

Directionally, thinner webs have been developed to reduce substrate mass, thereby improving light off performance, and to reduce pressure drop. High cell densities are developed to provide high geometric surface area for improved emission performance and precious metal utilization. High cell densities also provide mechanical strength, especially for ultra-thin walls. Correlations of bare (uncoated) substrate geometry have been developed to help explain the relationship between cell density and web thickness to emission performance and pressure drop (1,2). However, the presence of the washcoat and catalyst modifies the geometry and properties of the composite catalyst-substrate system. Correlations of coated substrate properties with performance are fewer, and generally first principle reaction engineering models have been used instead to understand the emission performance of catalyzed substrates (3).

EXPERIMENTAL BACKGROUND

SAMPLE SELECTION

A set of cordierite ceramic substrates were tested, spanning the range of cell densities and web thicknesses currently manufactured by Corning Incorporated. A summary of relevant properties of the bare substrates are shown in Table 1. Identical round substrates of 4.16” (105.7 mm) diameter by 3” long (76.2 mm) were packaged two to a can, and tested in a close-coupled location.

Table 1 Bare Substrate Properties

Product cpsi / web	Bulk Density g / L	OFA %	GSA cm^2/cm^3	Hydraulic Diameter mm
350 / 5.5	317	80.5	26.4	1.22
400 / 3	219	86.5	29.3	1.18
400 / 4	279	82.8	28.7	1.16
400 / 6	395	75.7	27.4	1.10
600 / 2	223	88.1	36.2	0.97
600 / 3	267	83.6	35.3	0.95
600 / 4	338	79.2	34.3	0.92
900 / 2	271	85.6	43.7	0.78

Substrates were coated with a modern washcoat formulation by a commercial coater. The precious metal was a Pd/Rh combination having a target 195 g/ft^3 loading, typical of some SULEV formulations.

EMISSIONS TEST PROCEDURES

Catalysts were aged separately from the test vehicle using a CARB rapid aging test-A procedure, described previously (4).

A 2 liter 4-cylinder multi-port fuel injected SULEV vehicle was tested in this study, using a 48" chassis dynamometer. The FTP-75 test cycle and measurement protocol was used. In addition, emissions measurements were taken continuously before and after the close-coupled converter. Excellent agreement was found between the three bag data and the integration of modal data from the continuous analyzers over the corresponding time period. Further details about the vehicle, catalyst aging and test setup used in this study can be found previous work (4).

FTP tests were run in triplicate to improve data quality. In most cases, two separate catalyzed samples were tested for each cell density and web thickness combination. This was done to improve statistical value and account for normal variations in sample preparation.

Emissions data were analyzed using the Minitab statistical software package. Regression analyses were performed on each component of the data; bag 1-3, integrated modal data, and subsets of the modal data.

EMISSIONS RESULTS

LIGHT-OFF FACTOR (LOF)

A light-off factor is defined in the Appendix for bare substrates as;

$$LOF = \frac{B \bullet GSA}{M^* \bullet D_h}$$

Where

$B = a\ constant$

$GSA = geometric\ \ surface\ \ area,\ \ cm^2/cm^3$

$M^* = heat\ \ capacity,\ \ cal/cm^3 \cdot K$

$D_h = channel\ \ hydraulic\ \ diameter,\ \ cm$

A regression analysis of the integrated modal hydrocarbon emissions over the first phase of the FTP-75 ("Phase-1", 0-505 seconds) versus the bare substrate light off factor is shown in Figure 1, for all substrates and replicate measurements. A reasonably good correlation is apparent, indicating that higher LOF leads to lower hydrocarbon emissions. Since all catalysts in these tests came to operating temperature within the first 60 seconds of the drive cycle, the Phase-1 data includes the true cold-start performance of each substrate combined with performance of the hot catalyst. After the catalysts come to operating temperature, other factors, especially available surface area (GSA in this study) become more dominant contributors to catalyst differentiation, and light-off related thermal mass and heat capacity less so.

Figure 1 Correlation of FTP Phase-1 HC Performance with Bare Substrate LOF

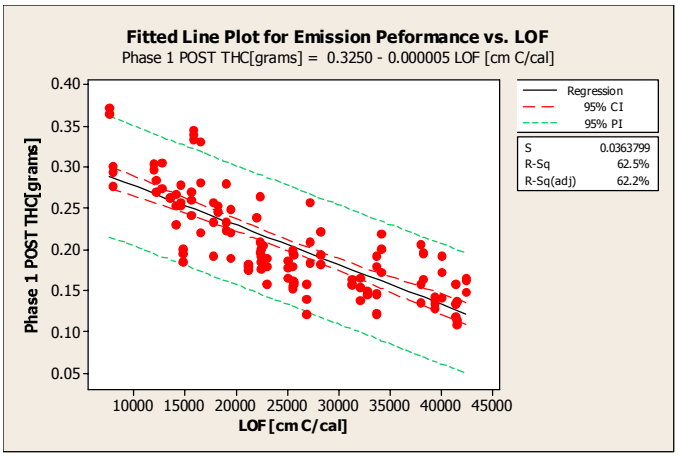

A similar type of regression analysis was performed for phases 2 and 3 of the drive cycle. As expected, the correlation with LOF is not as strong for these later stages of the FTP test since light off performance is not a primary factor after the catalyst becomes fully operational. Data scatter is also a consequence of the relatively low concentration of hydrocarbon in the later stages of the drive cycle. Figure 2 shows the correlation for the 3rd phase of the test, representing bag 3 and the last 505 seconds. The correlation coefficient, R^2, is poor.

Figure 2 Correlation of FTP Phase-3 HC Performance with Bare Substrate LOF

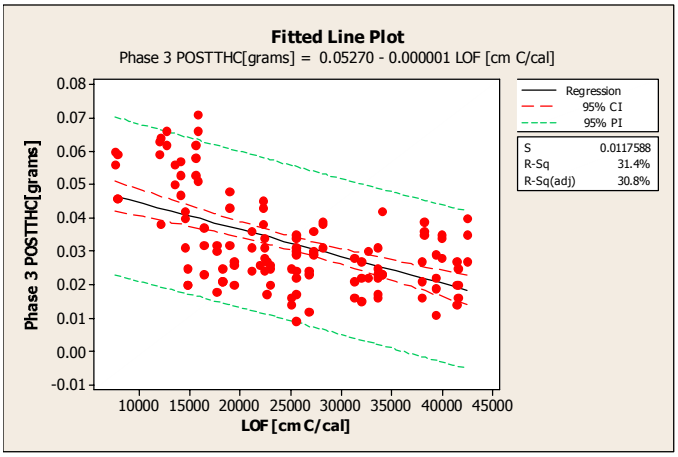

COATED LOF

A coated LOF can also be defined, analogous to bare, by substituting coated geometric properties;

$$LOF_{coated} = \frac{B \bullet GSA_{coated}}{M^{*}_{coated} \bullet D_h^{coated}}$$

Here we assumed that the heat capacity of the composite washcoat-substrate product is the same as cordierite, which is a reasonable approximation for high alumina content coatings (5). The linear regression of coated LOF versus Phase-1 data is shown in Figure 3. The quality of this correlation is comparable to that for the bare substrate LOF.

Figure 3 Correlation of FTP Phase-1 HC Performance with Coated Substrate LOF

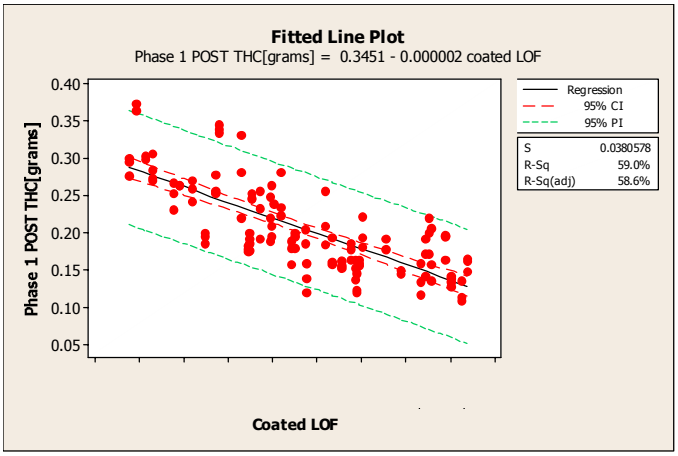

A comparison of the bare and coated LOF shows that they are highly correlated. This is related to the dominant effect of the bare substrate properties and indicates that either LOF can be used effectively. An improved coated LOF model would need to take into account thermal mass effects of the coating, the catalytic activity of the precious metals, and the exothermic heat release of the oxidation reactions.

Figure 4 Cross-Correlation of Coated and Bare LOF for FTP Phase-1 HC

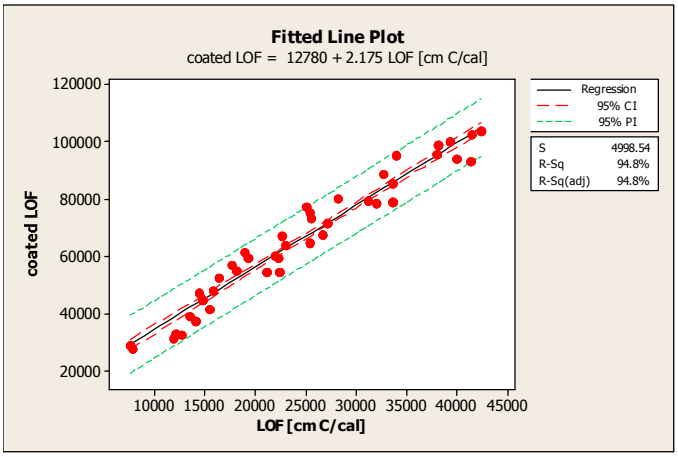

After averaging the emissions data for each nominal cell density and web thickness product, further correlations can be done to describe the impact of cell geometry on emission performance. Figure 5 shows a good relationship between the FTP-75 Bag 1 hydrocarbon quantity and the LOF_{coated} for various substrate products.

Figure 5 Correlation of FTP Phase-1 HC Performance

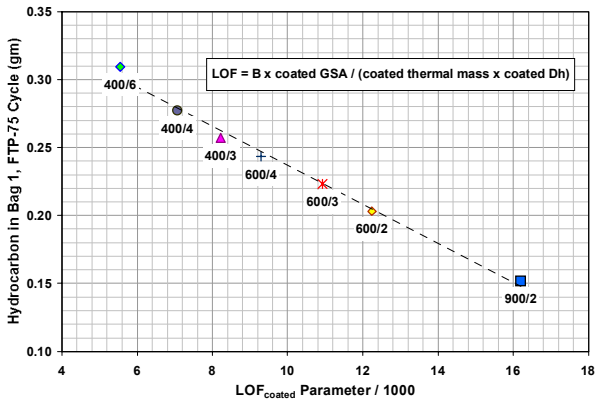

CONVERSION EFFICIENCY FACTOR (CEF)

The conversion efficiency factor for bare substrates was defined by Gulati as (1);

$$CEF = \frac{Nu \bullet GSA}{D_h}$$

CEF is similar to the LOF factor with the exception that does not account for thermal mass (M*) in the equation. This is related to the fact that the heat up of the catalyst is not relevant for steady state conversion efficiency (assumes that the catalyst has reached temperature equilibrium).

Figure 6 shows the correlation observed in the experimental data for total accumulated hydrocarbon in Phase-1 versus the CEF.

Figure 6 Correlation of Phase-1 HC Performance with Bare Substrate CEF

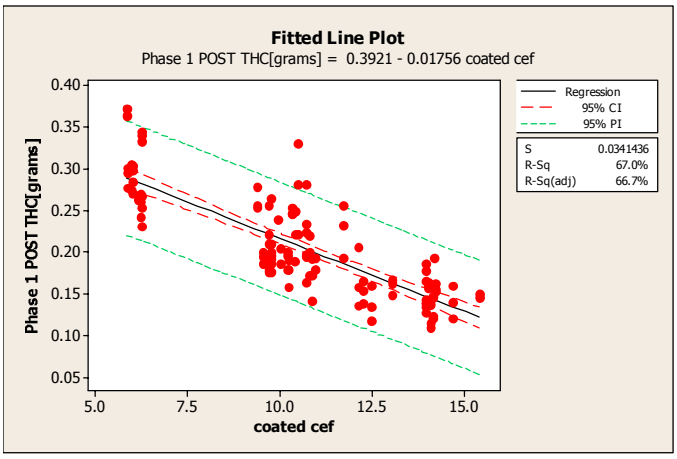

The linear regression in Figure 7 demonstrates the correlation observed in the experimental data for HC conversion over the total FTP-75 cycle versus the CEF.

Figure 7 Correlation of FTP-75 Performance with Bare Substrate CEF

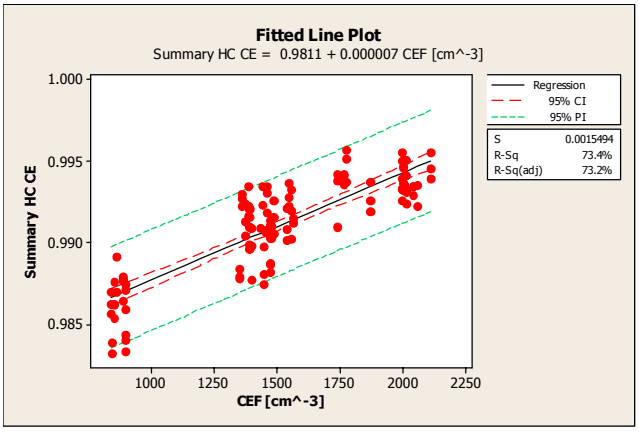

In general the CEF factor is good predictor of HC conversion performance over this drive cycle, with GSA being the dominant contributor.

PRESSURE DROP

Cold-flow pressure drop on bare substrates was measured on a conventional flow bench using compressed air at room temperature. Results are shown in Figure 8 as a function of flow rate. Reducing cell density has a major impact on observed pressure drop. Within a cell family, reducing web thickness has a secondary effect in reducing pressure drop. In both cases, the hydraulic diameter of individual channels is affected.

Figure 8 Cold-Flow Pressure Drop for Bare Substrates

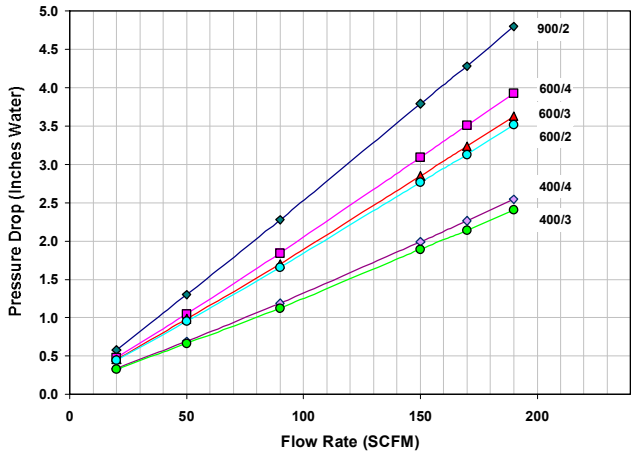

The pressure drop data can be combined with averaged emission performance data for each cell density and web thickness product to better understand the tradeoffs in these two critical performance measures. Figure 9 plots the cold-flow pressure drop data versus the FTP-75 predicted cumulative HC emissions for each product tested here. The bubble size in the plots is proportional to the calculated bare substrate LOF.

Figure 9 Pressure Drop vs. FTP-75 HC Emissions

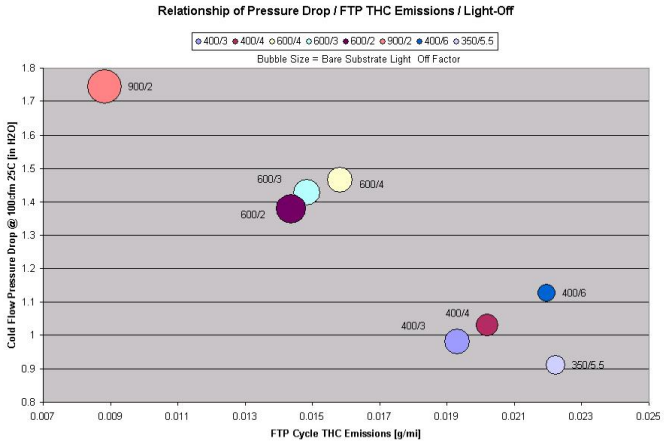

From this plot, the benefits of moving to thinner webs for both pressure drop reduction and emission performance are apparent. Also apparent is the impact of geometric surface area on the emissions performance. 900/2 has the highest GSA and therefore the lowest hydrocarbon emission level.

MECHANICAL STRENGTH CORRELATIONS

CELL STRUCTURE

Emission performance advantages of ultra-thin walled substrates are a consequence of the cell geometry. However as cell density and web thickness are reduced, mechanical strength decreases. A common method of assessing the axial tensile strength of cellular substrates is by a beam bending modulus of rupture (MOR) test. Typically the measurement of MOR stress makes use of an effective homogenous material assumption and ignores the cellular structure present within the test specimen (6). Although this homogenous material assumption simplifies test measurements and bulk material comparisons, it is not practical for cell density or wall thickness optimization in design work. Substituting the second area moment of the effective MOR beam cross section with that of the actual cellular cross section, allows for computation of the cellular wall scale stress, Figure 10.

Figure 10 Cellular Structure (left) vs. Effective Homogeneous Material (right) MOR Bar Cross-Section

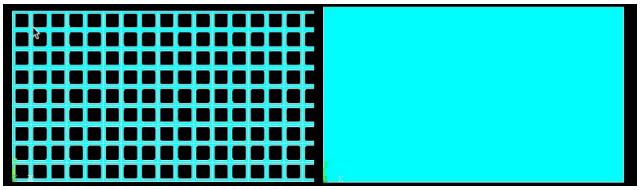

The widely known general beam bending equation for stress is given by (7):

$$\sigma = \frac{M \cdot c}{I}$$

Where;

$\sigma = bending\ \ stress$

$M = applied\ \ moment$

$c = distance\ \ from\ \ neutral\ \ axis$

$I = second\ \ area\ \ moment\ \ (moment\ \ of\ \ inertia\ )$

In the case of 4-point bending of a rectangular cross section, several key parameters can be given:

$$M = \frac{F(d_s - d_l)}{4}$$

$$c = \frac{W}{2}$$

$$I_b = \frac{W \cdot H^3}{12}$$

$$\sigma_{solid\_bar} = \frac{M \cdot c}{I_b}$$

Where;

$F = applied\ force$

$d_s = support\ span$

$d_l = load\ span$

$W = beam\ width$

$H = beam\ height$

$I_b = second\ area\ moment\ rectangular\ cross\ section\ bar$

$\sigma_{solid\ bar} = bending\ stress\ in\ a\ solid\ cross\ sectional\ bar$

If a cellular cross section replaces the assumption of a solid bar, I_b needs to be adjusted accordingly to account for the honeycomb shape (7).

$$I_c = I_b - I_{open\_channels}$$

$$I_c = \frac{W \cdot H^3}{12} - \frac{mn(p-t)^4}{12} + \frac{mp^2(p-t)^2}{4}\sum_{i=1}^{n}(2i-n-1)$$

$$_{web} = \frac{M \cdot c}{I_c}$$

$$_{bar_{web}} = _{web}(1 - OFA)$$

Where;

$I_c = second\ \ area\ moment,\ cellular\ \ bar,\ square\ channels$

$m = number\ \ of\ \ channels,\ width\ \ direction$

$n = number\ \ of\ \ channels,\ height\ \ direction$

$p = cell\ \ pitch,\ 1/cpsi^{0.5}$

$OFA = open\ \ frontal\ \ area$

$\sigma_{web} = bending\ \ stress\ at\ the\ cellular\ \ web\ scale$

$\sigma_{bar\ web} = bending\ \ stress,\ effective\ \ solid\ \ bar$

Given these expressions one can perform a parametric study comparing the relative effective bar strength of varying cell density and wall thickness. This can be accomplished by holding the predicted web stress at the cellular scale constant, and assuming a constant base material (e.g. cordierite at a given porosity) across all designs. While this could be solved algebraically, an iterative scheme varying the applied load was chosen in this study.

A constant web scale stress (σ_w) can be used as a surrogate for constant web material strength, therefore the effective homogeneous MOR bar stress (σ_b) can be solved as a function of cell density and web thickness. Figure 11 shows the results of such a simulation.

It should be noted that the absolute values in Figure 11 are not necessarily relevant for the purpose of this paper; instead this figure shows the relative difference between designs. For example, an 800 CPSI / 8 mil cell structure has a relative strength of 0.4 while a 600 CPSI / 2 mil substrate has a relative strength of 0.1. By ratio, there is a four-fold strength advantage to the 800/8 design based solely on the cellular design.

Figure 11 Relative Strength of Varying Web Thickness and Cell Density

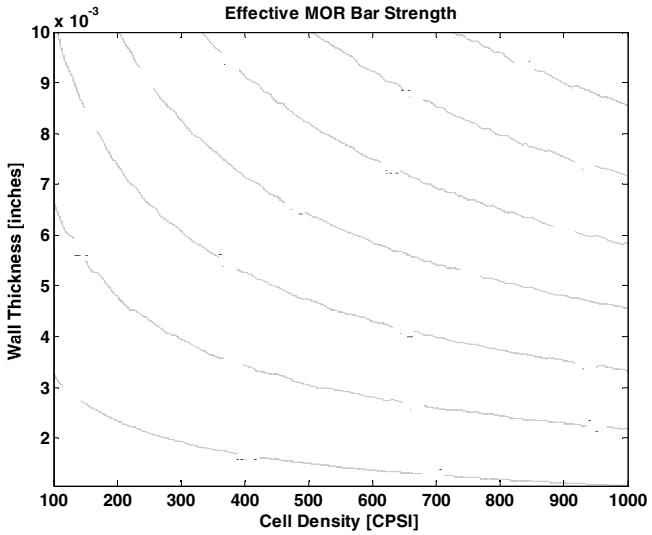

Similar plots can be made of other design parameters such as mechanical integrity factor (MIF), open frontal area (OFA), or bulk density (1, 2). The mechanical integrity factor;

$$MIF = \frac{t^2}{L \cdot (L - t)}$$

is a classic parameter which is very easy to calculate and has been used to quantify relative strength in cellular products. The methods described in this paper show MIF and MOR effective strength are strongly correlated as shown in Figure 12.

Figure 12 Relationship of Strength to MIF

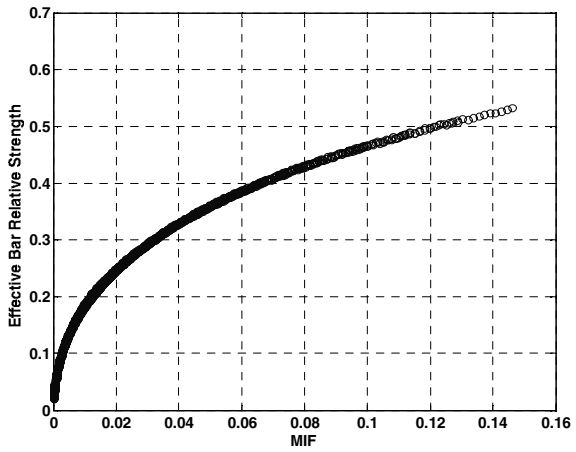

As expected, MIF increases in magnitude as the effective MOR strength increases. However it can be seen that the correlation is non-linear; therefore a 50% increase in MIF does not necessarily indicate a 50% increase in MOR bulk strength.

Similarly, effective MOR strength can be correlated to the relative bulk density for a given substrate design and material as shown in Figure 13. Here the closed frontal area (CFA) is used as a surrogate of bulk density since:

$$CFA = 1 - OFA$$

$$\rho_{bulk} = CFA \cdot \rho_{web}$$

Figure 13 Relative Strength vs. Closed Frontal Area

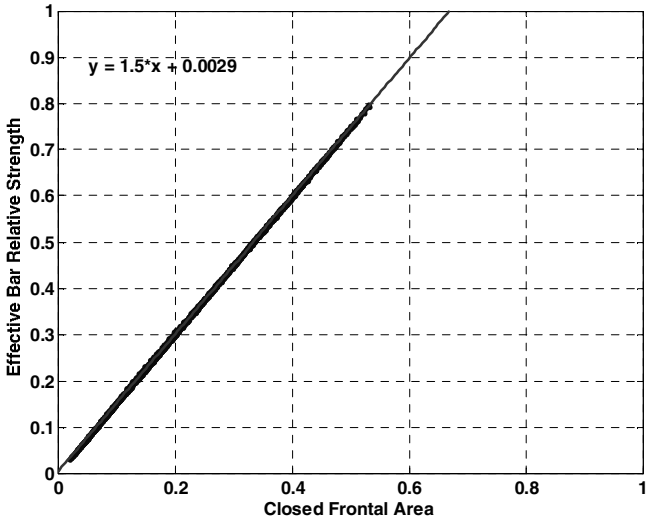

It is apparent from Figure 13 that the effective bar strength is directly proportional to CFA or bulk density and inversely proportional to OFA.

Finally, Gulati (1) has reported that MOR strength is also proportional to 2*t/L. Figure 14 shows that this simplified relationship is quite effective and gives a nearly linear correlation between methods.

Figure 14 Relative Strength vs. Web Thickness & Pitch

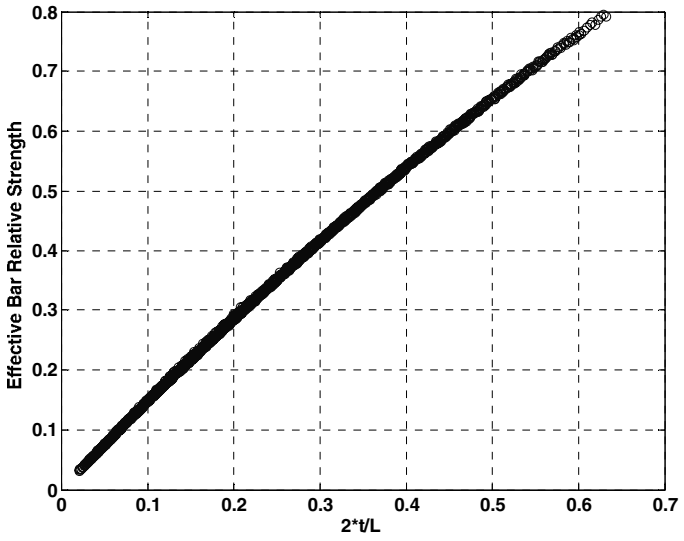

POROSITY

Another important factor determining the effective strength of a ceramic honeycomb product is the porosity of the webs. A well-known empirical relationship for strength in porous materials is given by the exponential Kingery relationship (1):

$$\sigma_w = \sigma_o e^{-bP}$$

Where;

$$\sigma_w = web\ strength$$
$$\sigma_o = dense\ material\ strength$$
$$b = empirical\ constant$$
$$P = porosity$$

The ratio of material strength at the web-scale for two different porosities can be expressed by:

$$\frac{\sigma_{P_2}}{\sigma_{P_1}} = \sigma_o e^{-b(P_2 - P_1)}$$

The dense material strength σ_o is a constant for a given material. Knowing this value and the b constant allows one to calculate the strength of several substrate geometries. Cordierite based materials are reported to have a b-constant near 5 (8).

Figure 15 shows how the ratio of material strength varies as a function of the porosity difference between two products. With increasing porosity, the material strength decreases exponentially.

Figure 15 Relationship of Strength to Web Porosity

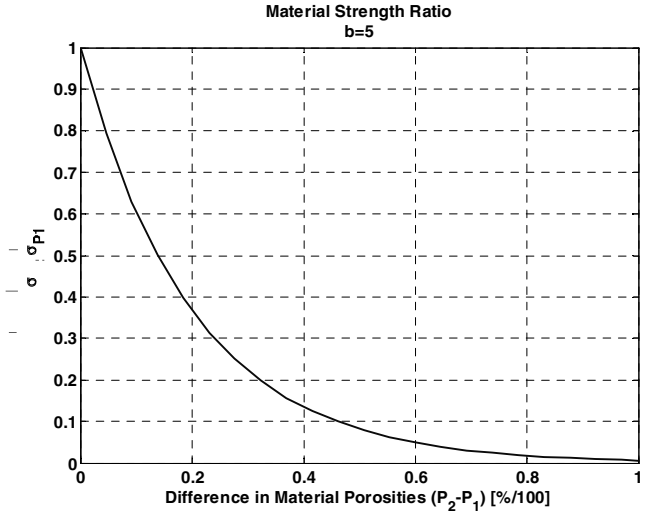

Figure 16 shows a plot of Phase-1 hydrocarbon performance versus the mechanical integrity factor. There is no theoretical reason to link mechanical strength with emissions performance, and Figure 16 is not meant to imply that there is a functional relationship. Instead, the plot illustrates the general trend that thinner web substrates products improve emission performance, especially in the cold-start phase, but do so at the expense of mechanical strength. Despite the lower strength of thinner webs, all of these products have been commercially accepted and used in applications. In some cases, improved canning and packaging technologies have been employed (9).

Figure 16 FTP Phase-1 HC vs. MIF

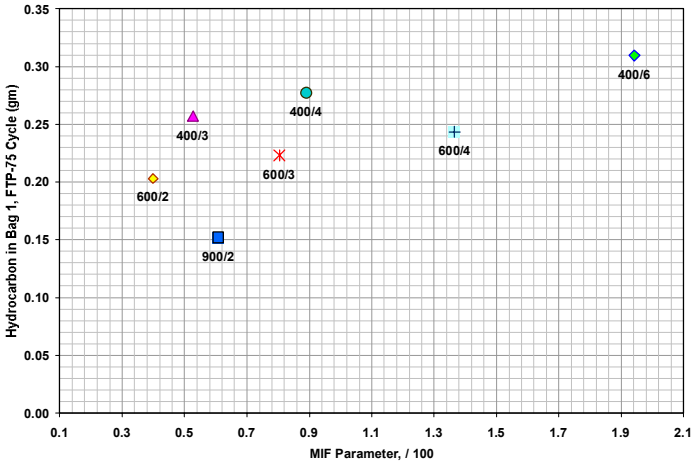

CONCLUSION

The effect of web thickness on emission performance, pressure drop, and mechanical properties was investigated for a series of catalyzed ceramic monolith

substrates having cell densities of 900, 600 and 400 cpsi. Thinner webs provide better catalyst light off performance and lower pressure drop, but mechanical strength generally decreases as web thickness is reduced. Phase-1 hydrocarbon emissions results from the FTP-75 drive cycle correlated well with a theoretical light-off factor, derived from cellular ceramic geometric parameters and simplified energy balance. An experimentally derived relationship between pressure drop and FTP-75 Bag-1 emissions shows a linear relationship with light off factor, and the relative ranking of commercially available cell density and web thickness substrates.

Mechanical strength estimates were used to understand cellular ceramic MOR bending stress and its relationship to cell density and web thickness. Additional correlations of MOR with geometric parameters and material porosity were presented. In general, reduction of web thickness reduces pressure drop, and improves light-off, but mechanical strength is reduced. Consideration of emission performance, pressure drop, mechanical strength, packaging, and overall cost are required for substrate design.

The data and results reported in this paper are based on tests conducted using certain apparatus and conditions with specific vehicles, systems, components, coatings, catalysts, and controls. Performance in other applications may differ based on conditions, apparatus, and other factors, including, but not limited to, the vehicles, systems, components, coatings, catalysts, and controls used.

ACKNOWLEDGMENTS

The authors wish to thank the scientists and technicians in the Product Development and Samples Development organizations in Corning for preparing samples of the numerous substrates tested in this project.

REFERENCES

1. Gulati, Suresh T., "Performance Parameters for Advanced Ceramic Catalyst Supports" SAE 1999-01-3631

2. Gulati, S.T., "Design Considerations for Advanced Ceramic Catalyst Supports", SAE 2000-01-0493

3. Tischer, S., Jiang, Y., Hughes, K.W., Patil, M.D., Murtaugh, "Three-Way Catalyst Modeling A Comparison of 1D and 2D Simulations", SAE 2—7-01-1071

4. Hughes, K.W., Gian, D., Calleja, J, "Relative Benefits of Various Cell Density Ceramic Substrates in Different Regions of the FTP Cycle", SAE 2006-01-1065

5. Day, J.P., "Substrate Effects on Light Off – Part 1 Thermal Energy Requirements", SAE 962074, SAE International Fall Fuels & Lubricants Meeting and Exposition, October 14, 1996

6. Wilcox, D., et al, "Predicting Thermal Stress in Diesel Particulate Filters", 2004 Diesel Engine Emissions Reduction (DEER) Conference Presentations, August 29-September 2, 2004 Coronado, California

7. Webb, J. E., et al, "Strength Size Effects in Cellular Ceramic Structures" Ceramic Engineering and Science Proceedings, Vol. 27; No. 2; pp. 521-532; October 2006

8. Gulati, S.T., "Durability and Performance of Thin Wall Ceramic Substrates", Symposium on International Automotive Technology (SIAT'99), SAE 990011, Jan. 1999

9. Eisenstock, G., et al, "Evaluation of SoftMount SM technology for use in packaging ultra thinwall ceramic substrates" SAE 2002-01-1097

APPENDIX – LIGHT OFF FACTOR DERIVATION

Assuming a radially uniform distribution of flow and temperature of gas into the substrate, no chemical reaction heat release, and an adiabatic system with respect to radial heat transfer to the surroundings (e.g. mat & can), an energy balance describing the heat-up of a single channel inside a honeycomb substrate can be written;

$$(1-OFA) \quad {}_s c_{p,s} \quad \frac{T_s}{t} =$$

$$(1-OFA) \quad {}_s \quad \frac{{}^2 T_s}{z^2} - \frac{Nu(z) \quad {}^g}{D_h} \quad GSA \quad (T_s - T_g)$$

Equation A 1

This equation can be simplified by assuming a constant Nusselt number, independent of time and location, constant gas conductivity, and that axial conduction in the solid is negligible.

Equation A1 then is reduced to;

$$(1-OFA) \cdot {}_s c_{p,s} \cdot \frac{dT}{dt} = - \frac{Nu \cdot {}^g}{D_h} \cdot GSA \cdot (T_s - T_g)$$

Equation A 2

Or alternatively;

$$\frac{dT}{dt} = \frac{-Nu \cdot \lambda_g \cdot GSA}{D_h \ (1-OFA) \ \rho_s \ c_{p,s}} \cdot (T_s - T_g)$$

Equation A 3

We define the light off factor, LOF as;

$$LOF = \frac{Nu \cdot \lambda_g \cdot GSA}{(1-OFA) \ \rho_s \ c_{p,s} \ D_h}$$

Equation A 4

Or to simplify;

$$LOF = \frac{B \ GSA}{M^* \cdot D_h}$$

Equation A 5

Where;

$$B = Nu \cdot \lambda_g$$

$$M^* = (1-OFA) \cdot \rho_s \cdot c_{p,s}$$

Glossary

$Nu = Nusselt\ number$

$\lambda_g = exhaust\ gas\ thermal\ conductivity, \frac{W}{m\ K}$

$T_s = substrate\ temperature, K$

$T_g = exhaust\ gas\ temperature, K$

$\rho_s = substrate\ bulk\ density, \frac{g}{cm^3}$

$c_{p,s} = substrate\ heat\ capacity, \frac{W}{g\ K}$

$t = time, s$

$z = axial\ distance\ down\ substrate\ channel, cm$

$D_h = channel\ hydraulic\ diameter, cm$

$GSA = geometric\ surface\ area, \frac{cm^2}{cm^3}$

$OFA = open\ frontal\ area$

$GSA_{coated} = washcoated\ substrate\ GSA$

$D_h^{coated} = washcoated\ substrate\ channel\ diameter$

$M^*_{coated} = washcoated\ substrate\ heat\ capacity$